Oxygen atom transfer in the reaction between hexakis(dimethyl-tert-butylsiloxy)ditungsten and nitric oxide. A remarkable difference in the reactivity of the tungsten–tungsten triple bond as a function of the attendant ligands: Bu^tO versus Bu^tMe_2SiO

Malcolm H. Chisholm*, Cindy M. Cook, Kirsten Folting and William E. Streib
Department of Chemistry and Molecular Structure Center, Indiana University, Bloomington, IN 47405 (USA)

Abstract

The siloxy complex $W_2(OSiMe_2Bu^t)_6$ (**I**) and NO react in hydrocarbon solvents in the presence of pyridine (py) to give the oxo tungsten compounds $W(O)(OSiMe_2Bu^t)_4(py)$ (**II**), $W_2(O)_4(OSiMe_2Bu^t)_4(py)_2$ (**III**) and $W(NO)(OSiMe_2Bu^t)_3(py)_2$ (**IV**). The relative amounts of the oxo compounds **II** and **III** to the nitrosyl complex **IV** depends upon the reaction temperature with low temperatures (−72 °C) favoring the nitrosyl derivative **IV**. An intermediate in the reaction is formulated as $W_2(\mu\text{-}O)(OSiMe_2Bu^t)_6(py)_2$ and is formed along with N_2O after the coupling of two nitrosyl ligands. The N_2O liberated in the reaction is then also active in oxygen atom transfer to yield **II** and **III** along with N_2. Compounds **II**, **III** and **IV** are inert with respect to further reactions with NO and N_2O under the conditions leading to their formation. An alternative synthesis of **IV** involves the reaction between $W(NO)(OBu^t)_3(py)$ and Bu^tMe_2SiOH (3 equiv.) in the presence of pyridine. Compounds **II**, **III** and **IV** have been characterized by single crystal X-ray crystallography, ^1H and ^{13}C NMR spectroscopy, IR spectroscopy and elemental analysis. Reactions employing $^{15}N^{18}O$ have been monitored by ^{15}N NMR spectroscopy and the products analyzed by mass spectrometry and IR spectroscopy. Compound **II** contains a distorted octahedral geometry about tungsten with *trans* oxo and pyridine ligands: W≡O = 1.68(1), W–O(siloxide) = 1.90(1) (av.), W–N = 2.44(1) Å. Compound **III** involves an edge-shared bioctahedron with terminal and bridging oxo ligands: W–O(oxo) = 1.72(1), W–μ-oxo = 1.95(1) (av.), W–O(siloxide) = 1.89(1) (av.) and W–N = 2.42(1) Å. Compound **IV** is pseudo-octahedral with *trans* nitrosyl and pyridine ligands: W–N(nitrosyl) = 1.74(1), W–N(pyridine-*trans*) = 2.34(1), W–N(pyridine-*cis*) = 2.29(1), W–O = 1.59(1) (av.) Å. A derivative of the intermediate $W_2(\mu\text{-}O)(OSiMe_2Bu^t)_6(py)_2$ was characterized by X-ray crystallography as $W_2(\mu\text{-}O)(\mu\text{-}OBu^t)(OSiMe_2Bu^t)_5(py)_2$ (**V**). Compound **V** contains bridging oxo and t-butoxide ligands that span a formal tungsten–tungsten double bond, W–W = 2.488(1) Å. In contrast to the above $Mo_2(OSiMe_2Bu^t)_6$ (**VI**) (made by the addition of Bu^tMe_2SiOH (6 equiv.) to $Mo_2(OBu^t)_6$) and NO (>2 equiv.) react in hydrocarbon solutions to give $[Mo(NO)(OSiMe_2Bu^t)_3]_2$ (**VII**), an analogue of the previously structurally characterized compound $[Mo(NO)(OBu^t)_3]_2$ that contains a centrosymmetric $(ON)(O_2M(\mu\text{-}O)_2MO_2(NO)$ skeleton with a linear M–N–O moiety and no M---M bond. Crystallographic data for the compounds: **II**: space group $P\bar{1}$, $a = 17.414(5)$, $b = 22.679(7)$, $c = 11.519(3)$ Å, $\alpha = 99.77(2)$, $\beta = 102.15(2)$, $\gamma = 108.13(1)°$, $V = 4089.00$ Å^3, $Z = 4$; **III**: space group $P\bar{1}$, $a = 10.708(3)$, $b = 12.469(4)$, $c = 10.185(3)$ Å, $\alpha = 107.44(1)$, $\beta = 111.56(1)$, $\gamma = 90.53(2)°$, $V = 1195.75$ Å^3, $Z = 1$; **IV**: space group $P2_1/c$, $a = 14.049(3)$, $b = 10.832(2)$, $c = 24.807(5)$ Å, $\beta = 102.00(1)°$, $V = 3692.74$ Å^3, $Z = 4$; **V**: space group $P\bar{1}$, $a = 14.881(3)$, $b = 17.245(3)$, $c = 12.830$ Å, $\alpha = 91.20(1)$, $\beta = 102.23(1)$, $\gamma = 76.34(1)°$, $V = 3125.26$ Å^3, $Z = 2$.

Introduction

We have now established a fairly extensive body of chemistry for the compounds $M_2(OR)_6(M{\equiv}M)$ where M = Mo and W [1]. These provide templates for organometallic chemistry and the presence of the dinuclear, redox-active metal center often affords modes of ligand binding and reactivity not seen in mononuclear chemistry [2]. Reactions involving alkynes have led to the formation of alkyne adducts in which there is a central pseudo-tetrahedral $W_2(\mu\text{-}C_2R_2)$ moiety [3], products derived from C–C coupling such as $M_2(\mu\text{-}C_4R_4)$ containing compounds [4], or products derived from metathesis of the M≡M and C≡C functionalities [5]. In the case of the reaction between $W_2(OBu^t)_6$ and C_2H_2 in hydrocarbon solvents a $W_2(\mu\text{-}C_4H_4)(OBu^t)_6$ compound is formed by way of a reactive $W_2(\mu\text{-}C_2H_2)(OBu^t)_6$ intermediate. The latter can be isolated as a pyridine adduct, $W_2(\mu\text{-}C_2H_2)(OBu^t)_6(py)$, which adopts structure **A**.

*Author to whom correspondence should be addressed.

0020-1693/92/$5.00

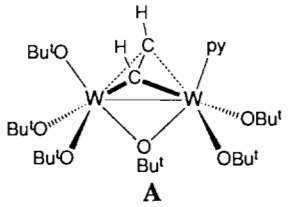

A

In solution $W_2(\mu\text{-}C_2H_2)(OBu^t)_6(py)$ is labile to alkyne coupling and also exists in an equilibrium involving the methylidyne complex $(Bu^tO)_3W{\equiv}CH$ according to eqn. (1) [3].

$$W_2(\mu\text{-}C_2H_2)(OBu^t)_6(py) \longrightarrow 2[(Bu^tO)_3W{\equiv}CH] + py \quad (1)$$

We became interested in how subtle changes in the spectator ligands could influence the reactivity of the M≡M bond and thus we have initiated a study of the chemistry of siloxides of formula $M_2(OSiR_3)_6$. The use of the sterically demanding Bu^tMe_2SiO ligand allows access to $M_2(OSiR_3)_6$ (M = Mo, W) compounds that do not require additional Lewis bases, i.e. in their unligated form they are persistent with respect to oligomerization [6].

The reactions between $W_2(OSiMe_2Bu^t)_6$ and ethyne are summarized in Scheme 1 [7] and are notably different from those cited above for $W_2(OBu^t)_6$. We would like to determine whether or not these differences in reactivity arise from steric or electronic effects associated with the spectator ligands Bu^tO versus Bu^tMe_2SiO. Our initial prejudice was that electronically the donor properties of the ligands $(\sigma+\pi)$ follow the order $Bu^tO > Bu^tMe_2SiO$ and furthermore that $^-OSiMe_2Bu^t$ is a better leaving group relative to $^-OBu^t$. In the latter regard the siloxide ligand may facilitate the migration of protons between reactive species more readily in processes like those shown in Scheme 1. As an interrogation of the relative donor properties of Bu^tO versus Bu^tMe_2SiO, we set out to prepare analogous nitrosyl complexes of equivalent structure and formula, e.g. $X_3W(NO)(py)$ where $X = Bu^tO$ and Bu^tMe_2SiO. In such compounds, the nitrosyl ligand provides an opportunity of comparing X_3W d_π-to-NO π^* backbonding in much the same way that a single carbonyl ligand is responsive to the π-donating properties of a metal fragment. As a good first approximation, the lower the value of ν(CO) or ν(NO) (linear nitrosyl), the greater the back donation from the metal.

The compound $W(NO)(OBu^t)_3(py)$ had been previously prepared from the reaction between $W_2(OBu^t)_6$ and NO (2 equiv.) in pyridine solution (eqn. (2)) [8].

$$W_2(OBu^t)_6 + 2NO \xrightarrow[py]{0\ ^\circ C} 2W(NO)(OBu^t)_3(py) \quad (2)$$

In this reaction the metal–metal bond is cleaved to yield two mononuclear tungsten nitrosyls. We set out to prepare the siloxy analogue to $W(NO)(OBu^t)_3(py)$ by reaction of **I** with NO and pyridine. This report gives the details of this reaction which yields oxygen atom transfer products as well as a tungsten nitrosyl compound.

Experimental

General methods

Standard air sensitive techniques were used throughout. Solvents used were dry and oxygen-free. Details of the techniques used in this laboratory and the

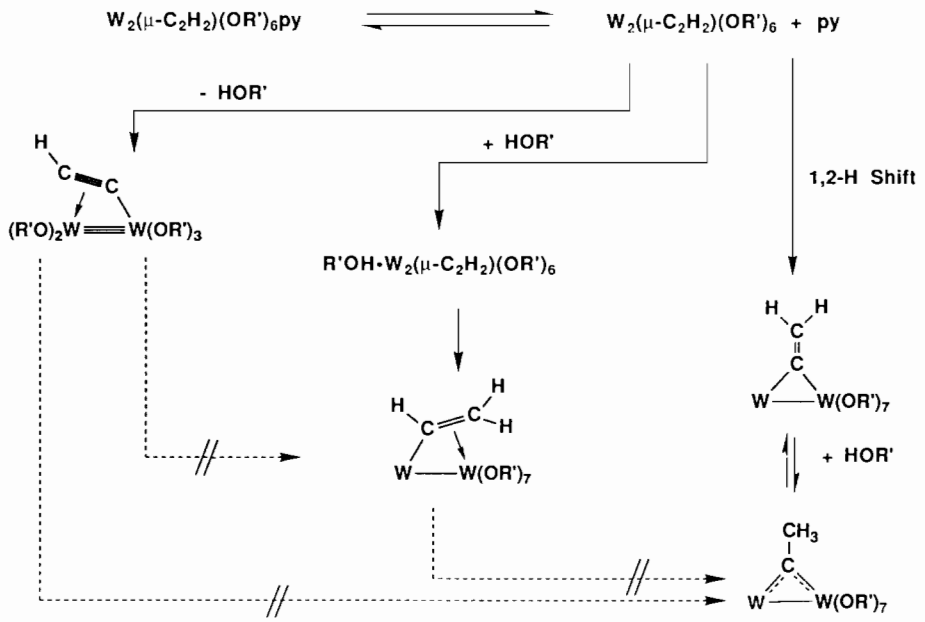

Scheme 1. H-atom transfer reactions involving $W_2(\mu\text{-}C_2H_2)(OSiMe_2Bu^t)_6(py)$ and $HOSiMe_2Bu^t$ where R' represents $SiMe_2Bu^t$.

preparation of $W_2(OBu^t)_6$ have been described previously [9]. Bu^tMe_2SiOH (Aldrich) was placed over 4 Å molecular sieves and freeze, thaw, degassed before use. Nitric oxide (MG Speciality Gas) and isotopically enriched nitric oxide (^{15}N, 99.9%; ^{18}O, 96.2%; Isotec) were used as received. $Mo_2(OBu^t)_6$ was prepared by a published method [10]. The literature preparation of $W(NO)(OBu^t)_3(py)$ [8] was modified by changing the reaction solution from neat pyridine to hexane/py (10:1).

Elemental analyses were performed by Oneida Research Services, Inc., New York. IR spectra were obtained on a Perkin-Elmer 283 spectrophotometer as Nujol mulls between CsI plates. ^1H NMR spectra were recorded on either a Varian XL-300 or a Nicolet-360 NMR spectrophotometer in dry and oxygen-free toluene-d_8 or benzene-d_6. ^1H NMR chemical shifts are in parts per million relative to the protio impurity in benzene-d_6 set at δ 7.15 or the CHD_2 quintet of toluene-d_8 set at δ 2.09. ^{13}C NMR spectra were recorded on a Varian XL-300 spectrophotometer at 75 MHz. ^{13}C chemical shifts are in parts per million relative to the triplet of benzene-d_6 set at δ 128.0.

The ^{15}N NMR spectra were obtained on a Nicolet 360 spectrophotometer operating at 36.6 MHz. The ^{15}N signal of nitromethane, CH_3NO_2, 1 M in $Cr(acac)_3$ set at δ 2.75 was used as the external reference. The reaction of **I** with $^{15}N^{18}O$ was carried out in a toluene (2.5 ml)/pyridine (0.5 ml) solvent mixture 0.03 M in $Cr(acac)_3$ in a 10 mm NMR tube.

Preparation of $W(O)(OSiMe_2Bu^t)_4(py)$ (II), $W_2(O)_4(OSiMe_2Bu^t)_4(py)_2$ (III) and $W(NO)(OSiMe_2Bu^t)_3(py)_2$ (IV)

Compound **I** (310 mg, 0.268 mmol) was dissolved in 5 ml toluene and 1 ml pyridine. The burgundy solution was frozen at −196 °C, the flask evacuated, and NO (0.804 mmol) was condensed into the flask via a calibrated manifold. The flask was immediately placed in a −30 °C cold bath with stirring. After 0.5 h the reaction solution was purple in color and faded to orange–yellow within 3 h. The volatiles were removed *in vacuo* leaving an orange–yellow powder. Cold finger sublimation at 60 °C and 10^{-4} torr isolated **II** as a white solid (62 mg, 29%). X-ray quality and analytically pure crystals of **II** were formed as colorless needles from concentrated toluene solutions at −20 °C. *Anal.* Calc. for $C_{29}H_{65}NO_5Si_4W$: C, 43.32; H, 8.15; N, 1.74. Found: C, 43.47; H, 8.04; N, 1.62%. ^1H NMR (benzene-d_6, 22 °C, 300 MHz): 9.90 (CH, *o*-py, 2H); 6.92 (CH, *p*-py, 1H); 6.68 (CH, *m*-py, 2H); 1.11 (CMe_3, 36H); 0.21 (Me_2, 24H). ^{13}C NMR (benzene-d_6, 22 °C, 75 MHz): 149.4 (CH, *o*-py); 138.0 (CH, *m*-py); 123.9 (CH, *p*-py); 27.2 (CMe_3); 26.2 (CMe_3); −2.1 (Me_2). IR (cm^{-1}, Nujol mull): 1599m, 1403m, 1245s, 1210m, 1150m, 1070m, 1033s, 1005s, 960–790s (br), 760s, 695s, 673s, 620m, 580w, 505m, 455m, 432m, 393m, 361s, 342s.

The sublimation residue from above was dissolved in toluene, concentrated *in vacuo* and 50 μl pyridine added. **III** was deposited as colorless, thin, needle-like crystals at −20 °C (32 mg, 20%). *Anal.* Calc. for $C_{34}H_{70}N_2O_8Si_4W_2$: C, 36.63; H, 6.33; N, 2.51. Found: C, 35.67; H, 6.07; N, 2.61%. ^1H NMR (benzene-d_6, 22 °C, 300 MHz): 8.78 (CH, *o*-py, 2H); 6.90 (CH, *p*-py, 1H); 6.68 (CH, *m*-py, 2H); 1.09 (CMe_3, 18H); 0.31 (Me_2, 12H). ^{13}C NMR (benzene-d_6, 22 °C, 75 MHz): 149.7 (CH, *o*-py); 123.7 (CH, *p*-py); 26.3 (CMe_3); 20.0 (CMe_3); −3.4 (Me_2), the *m*-py signal may be obscured by the solvent signals. IR (cm^{-1}, Nujol mull): 1599m, 1446s, 1411m, 1152w, 1068m, 1036m, 1011m, 972s, 932–920s, 840–810s, 830s, 818s, 800s, 771s, 750s, 718m, 691s, 672–662s, 620m, 580w, 536w, 488m, 400w, 393w, 358m.

The volatiles from the supernatant of **III** above were removed *in vacuo* and the orange powder resuspended in pentane. From a very concentrated solution, orange crystals of **IV** formed upon standing (63 mg, 15%).

Alternative synthesis of IV

$W(NO)(OBu^t)_3(py)$ (295 mg, 0.576 mmol) was placed in a Schlenk flask equipped with a stirbar. Pentane (10 ml) and pyridine (50 μl) were added with stirring, forming a yellow slurry. At 22 °C, $HOSiMe_2Bu^t$ (0.27 ml, 1.728 mmol) was added at once via syringe, immediately forming an orange solution. After 4 h the volatiles were removed *in vacuo* leaving an orange powder. The reaction was quantitative by ^1H NMR spectroscopy. Analytically pure and X-ray quality crystals of **IV** were grown from pentane solutions stored at −20 °C for 3 h. Combined crystallizations isolated **IV** in 79% yield (348 mg, 0.455 mmol). *Anal.* Calc. for $C_{28}H_{55}N_3O_4Si_3W$: C, 43.91; H, 7.24; N, 5.49. Found: C, 43.74; H, 7.10; N, 5.37%. ^1H NMR (benzene-d_6, 22 °C, 300 MHz): 9.24 (CH, *o*-py, 2H); 8.50 (CH, *o*-py, 2H); 6.89 (CH, *p*-py, 1H); 6.68 (overlapping CH, m, *p*-py, 3H); 6.38 (CH, *m*-py, 2H); 1.03 (CMe_3, 27H); 0.46 (Me_2, 18H). ^1H NMR (toluene-d_8, −60 °C, 360 MHz): 9.16 (CH, *o*-py, 2H); 8.38 (CH, *o*-py, 2H); 6.65 (CH, *p*-py, 1H); 6.48 (CH, *m*-py, 2H); 6.43 (CH, *p*-py, 1H); 6.12 (CH, *m*-py, 2H); 1.08 (CMe_3, 27H); 0.74 (Me_2, 6H); 0.64 (Me_2, 6H); −0.13 (Me_2, 6H). IR (cm^{-1}, Nujol mull): 1599s, 1548m, 1542s ($\bar{\nu}$(NO)), 1478s, 1400m, 1250s, 1245s, 1240s, 1211s, 1150w, 1141w, 1063m, 1038m, 1015m, 1008m, 980–860s(br), 828s, 797m, 768s, 758s, 691s, 675m, 638w, 608m, 568vw, 490w, 480w, 440vw, 385vw, 328w.

$Mo_2(OSiMe_2Bu^t)_6$ (VI)

Hexane (15 ml) was added via cannula to a Schlenk flask equipped with $Mo_2(OBu^t)_6$ (152 mg, 0.241 mmol) and a stirbar. At 22 °C, Bu^tMe_2SiOH (0.23 ml, 1.45

mmol) was added at once with stirring. After 10 min the solution color began to change from yellow–orange to orange–red. After 4.5 h the volatiles were removed *in vacuo*, leaving an orange–red solid. Analytically pure crystals of **VI** were grown from hexane at −20 °C in 82% isolated yield (193 mg, 0.197 mmol). *Anal.* Calc. for $C_{36}H_{90}Mo_2O_6Si_6$: C, 44.14; H, 9.26. Found: C, 44.15; H, 8.98%. ^{1}H NMR (benzene-d_6, 22 °C, 300 MHz): 1.01 (CMe_3, 9H); 0.37 (Me_2, 6H). ^{13}C NMR (benzene-d_6, 22 °C, 75 MHz): 26.5 (CMe_3); 19.6 (CMe_3); −1.3 (Me_2).

$Mo_2(NO)_2(OSiMe_2Bu^t)_6$ (VII)

Compound **VI** (507 mg, 0.518 mmol) was weighed into a Schlenk flask equipped with a stirbar. Pentane (10 ml) was added via cannula. The flask was frozen at −196 °C, evacuated and NO (1.56 mmol) added. The flask was immediately placed at −35 °C with stirring. After 10 min the orange color of the solution turned yellow and a yellow precipitate began to form. As the cold bath warmed to room temperature the reaction mixture became homogeneous. After 4 h the volatiles were removed *in vacuo* leaving a yellow crystalline solid. Yellow crystals of **VII** formed from toluene solutions at −20 °C and were isolated in two batches for a total yield of 88% (473 mg, 0.455 mmol). *Anal.* Calc. for $C_{36}H_{90}Mo_2N_2O_8Si_6$: C, 41.60; H, 8.73; N, 2.70. Found: C, 41.45; H, 8.72; N, 2.77%. ^{1}H NMR (benzene-d_6, 27 °C, 300 MHz): 1.08 (CMe_3, 9H); 0.49 (Me_2, 6H). ^{1}H NMR (toluene-d_8, −40 °C, 360 MHz): 1.16 (CMe_3, 9H); 1.08 (CMe_3, 18H); 0.56 (Me_2, 12H); 0.45 (Me_2, 6H). ^{13}C NMR (benzene-d_6, 27 °C, 75 MHz): 27.2 (CMe_3); 19.6 (CMe_3); −0.2 (Me_2). IR (cm^{-1}, Nujol mull): 1648 s ($\tilde{\nu}$(NO)), 1408m, 1255s, 1248s, 1160vw, 1148vw, 1113w, 1100w, 943m, 913–900s(br), 850–840s(br), 830s, 818s, 798s, 784s, 778s, 752s, 721s, 718s, 671m, 624w, 572w, 522w, 518w, 490w, 392vs, 358vw, 323vw.

$Mo(NO)(OSiMe_2Bu^t)_3(py)_2$ (VIII)

Toluene (6 ml) was added to a Schlenk flask containing **VII** (300 mg, 0.289 mmol) with stirring. The yellow color of the solution immediately changed to purple upon addition of pyridine (1 ml). The solution volume was reduced to 1 ml. After 5 min at 22 °C large rectangular purple crystals had formed. The elemental analyses are satisfactory for a compound of formula **VIII**·toluene or **VIII**·0.5 toluene. The ^{1}H NMR spectrum of the crystals shows free toluene and integration results best fit the formulation **VIII**·toluene. *Anal.* Calc. for $C_{35}H_{63}MoN_3O_4Si_3$ (**VIII**·toluene): C, 52.33; H, 8.65; N, 5.73. Found: C, 52.06; H, 8.29; N, 5.72%. Based on this formula, the isolated yield is 91% (405 mg, 0.526 mmol). ^{1}H NMR (benzene-d_6, 22 °C, 300 MHz): 9.12 (CH, *o*-py, 2H); 8.42 (CH, *o*-py, 2H); 7.03 (CH, *p*-py, 1H); 6.82 (CH, *m*-py, 2H); 6.67 (CH, *p*-py, 1H); 6.51 (CH, *m*-py, 2H); 1.04 (CMe_3, 27H); 0.39 (Me_2, 18H). ^{1}H NMR (toluene-d_8, −60 °C, 360 MHz): 9.16 (CH, *o*-py, 2H); 8.20 (CH, *o*-py, 2H); 6.56 (CH, *m*-py, 1H); 6.45 (CH, overlapping *p*-py, *m*-py, 3H); 6.06 (CH, *m*-py, 2H); 1.16 (CMe_3, 18H); 1.14 (CMe_3, 9H); 0.78 (Me_2, 6H); 0.67 (Me_2, 6H); −0.12 (Me_2, 6H). IR (cm^{-1}, Nujol mull): 1624s ($\tilde{\nu}$(NO)), 1598w, 1295w, 1248s, 1239s, 1209m, 1147w, 1063m, 1033m, 1008w, 970–960m(br), 890–879s(br), 827s, 795m, 765s, 750m, 720s, 715m, 689m, 615w, 628w, 610w, 485–475w(br), 380vw, 358w, 328vw.

Single crystal and molecular structure determination

General procedures have been described elsewhere [11]. A summary of crystal data and atomic coordinates are given in the Tables 1–9. Inert atmosphere handling

TABLE 1. Atomic positional parameters (×10^4) for **II**

Atom	*x*	*y*	*z*
W(1)	7427.4(2)	2596.9(1)	1966.9(3)
O(2)	7990(3)	2306(2)	2937(5)
N(3)	6654(4)	3032(3)	540(5)
C(4)	5836(5)	2757(4)	−6(8)
C(5)	5395(5)	2975(4)	−849(9)
C(6)	5811(6)	3512(5)	−1176(8)
C(7)	6662(6)	3808(4)	−631(9)
C(8)	7057(5)	3565(4)	228(7)
O(9)	7220(4)	3187(3)	3123(5)
Si(10)	6969(1)	3754(1)	3814(2)
C(11)	5899(6)	3687(5)	2975(9)
C(12)	7728(6)	4538(4)	3839(8)
C(13)	7018(5)	3679(4)	5431(8)
C(14)	6927(6)	4263(4)	6184(8)
C(15)	7859(6)	3628(4)	6021(8)
C(16)	6314(6)	3075(4)	5433(9)
O(17)	6332(3)	2002(2)	1755(5)
Si(18)	5578(1)	1397(1)	1891(2)
C(19)	5011(5)	873(4)	327(8)
C(20)	4840(6)	1704(5)	2523(9)
C(21)	6042(5)	958(4)	2925(7)
C(22)	6680(5)	733(4)	2438(8)
C(23)	5330(5)	368(4)	2992(8)
C(24)	6480(6)	1391(4)	4233(7)
O(25)	7438(4)	2121(3)	461(5)
Si(26)	7428(1)	1844(1)	−949(2)
C(27)	6373(6)	1646(5)	−2009(9)
C(28)	8199(6)	2467(4)	−1408(8)
C(29)	7728(5)	1111(4)	−988(8)
C(30)	6971(6)	528(4)	−1025(10)
C(31)	8430(5)	1229(4)	158(9)
C(32)	8013(7)	956(5)	−2129(9)
O(33)	8359(3)	3298(3)	1882(5)
Si(34)	9385(1)	3585(1)	2509(2)
C(35)	9820(5)	2952(4)	2108(8)
C(36)	9606(6)	3826(5)	4202(8)
C(37)	9864(5)	4294(4)	1909(8)
C(38)	9649(6)	4103(4)	508(9)
C(39)	9555(6)	4842(4)	2262(10)
C(40)	10822(6)	4542(4)	2428(9)

TABLE 2. Selected bond distances (Å) and angles (°) for **II**

Distances	
W(1)–O(2)	1.68(1)
W(1)–O(9)	1.90(1)
W(1)–O(17)	1.90(1)
W(1)–O(25)	1.89(1)
W(1)–O(33)	1.92(1)
W(1)–N(3)	2.44(1)
Si–O	1.63 (av)
Angles	
W(1)–O(9)–Si(10)	165.7(4)
W(1)–O(17)–Si(18)	160.5(3)
W(1)–O(25)–Si(26)	167.5(4)
W(1)–O(33)–Si(34)	135.5(3)
O(2)–W(1)–O(9)	99.5(2)
O(2)–W(1)–O(17)	99.1(2)
O(2)–W(1)–O(25)	99.4(2)
O(2)–W(1)–O(33)	97.0(2)
O(2)–W(1)–N(3)	178.1(2)
O(9)–W(1)–O(17)	88.8(2)
O(9)–W(1)–O(25)	161.3(2)
O(9)–W(1)–O(33)	88.2(3)
O(9)–W(1)–N(3)	81.4(2)
O(17)–W(1)–O(25)	88.8(3)
O(17)–W(1)–O(33)	163.9(2)
O(17)–W(1)–N(3)	82.6(2)
O(25)–W(1)–O(33)	89.0(3)
O(25)–W(1)–N(3)	79.9(2)
O(33)–W(1)–N(3)	81.3(2)

TABLE 3. Atomic positional parameters ($\times 10^4$) for **III**

Atom	*x*	*y*	*z*
W(1)	9763.6(3)	3765.9(2)	9023.3(3)
O(2)	8800(5)	5046(4)	9505(5)
O(3)	9860(5)	3833(4)	7403(5)
N(4)	9582(6)	3576(5)	11245(7)
C(5)	10664(7)	3493(6)	12394(8)
C(6)	10616(8)	3500(7)	13720(8)
C(7)	9387(9)	3590(7)	13898(9)
C(8)	8268(8)	3664(7)	12717(9)
C(9)	8409(8)	3649(7)	11422(8)
O(10)	8118(5)	2797(4)	8202(5)
Si(11)	6784(2)	2081(2)	6689(2)
C(12)	5839(8)	1130(7)	7202(10)
C(13)	7423(8)	1241(7)	5270(9)
C(14)	5677(7)	3126(7)	5984(9)
C(15)	4369(8)	2493(8)	4674(10)
C(16)	6449(9)	3845(9)	5461(11)
C(17)	5341(9)	3906(8)	7234(10)
O(18)	10957(5)	2674(4)	9382(5)
Si(19)	12156(2)	2020(2)	8966(2)
C(20)	12006(8)	1994(7)	7080(9)
C(21)	13818(8)	2823(8)	10383(10)
C(22)	11908(8)	536(7)	9042(8)
C(23)	11730(8)	627(7)	10488(9)
C(24)	10647(9)	−155(7)	7703(10)
C(25)	13156(9)	−45(8)	9027(11)

TABLE 4. Selected bond distances (Å) and angles (°) for **III** (primes refer to centrosymmetrically related atoms)

Distances	
W(1)–W(1)′	3.041(1)
W(1)–O(2)′	1.93(1)
W(1)–O(2)	1.95(1)
W(1)–O(3)	1.72(1)
W(1)–O(10)	1.88(1)
W(1)–O(18)	1.90(1)
W(1)–N(4)	2.42(1)
Si–O	1.65 (av)
Angles	
O(2)′–W(1)–O(2)	76.8(2)
O(2)–W(1)–O(3)	101.2(2)
O(2)′–W(1)–O(3)	100.8(2)
O(2)′–W(1)–O(10)	157.3(2)
O(2)–W(1)–O(10)	88.9(2)
O(2)′–W(1)–O(18)	89.4(2)
O(2)–W(1)–O(18)	157.4(2)
O(2)–W(1)–N(4)	80.5(2)
O(2)′–W(1)–N(4)	81.7(2)
O(3)–W(1)–O(10)	99.2(2)
O(3)–W(1)–O(18)	98.9(2)
O(3)–W(1)–N(4)	177.3(2)
O(10)–W(1)–O(18)	98.1(2)
O(10)–W(1)–N(4)	78.7(2)
O(18)–W(1)–N(4)	79.8(2)
W(1)′–O(2)–W(1)	103.2(2)
W(1)–O(10)–Si(11)	147.8(3)
W(1)–O(18)–Si(19)	145.2(3)

techniques were used until the crystals had been mounted and transferred to a cold stream on a goniostat. All intensity data were collected in the range $6 \leqslant 2\theta \leqslant 45°$ using continuous θ–2θ scans and Mo Kα radiation (0.71069 Å). The structures were solved by using direct methods (MULTAN78) [12] and Patterson and Fourier techniques. Hydrogen atoms were included in fixed calculated positions using idealized geometries and d(C–H) = 0.95 Å. Hydrogen thermal parameters were fixed at one plus the isotropic thermal parameter [13] of the atom to which they were bonded.

$W(O)(OSiMe_2Bu^t)_4(py)$ (II)

There are two molecules in the asymmetric unit. The non-hydrogen atoms are labelled W(1)–C(40) for the first molecule and W(41)–C(80) for the second. The final difference Fourier was reasonably clean. There were tungsten residuals of 0.75–1.37 e/Å^3. All other residual peaks were less than 0.75 e/Å^3.

$W_2(O)_4(OSiMe_2Bu^t)_4(py)_2$ (III)

The final difference map was reasonably clean with tungsten residuals of 1.0–2.1 e/Å^3. All other residual peaks were 0.8 e/Å^2 or less.

TABLE 5. Atomic positional parameters ($\times 10^4$) for **IV**

Atom	x	y	z
W(1)	3045.2(2)	2275.3(3)	6288.6(1)
O(2)	2312(4)	2575(5)	5560(2)
Si(3)	1841(2)	1849(2)	4980(1)
C(4)	1371(7)	302(9)	5139(4)
C(5)	2804(7)	1624(10)	4579(4)
C(6)	848(6)	2867(8)	4588(3)
C(7)	322(7)	2232(10)	4056(4)
C(8)	1299(7)	4095(9)	4450(4)
C(9)	98(7)	3157(9)	4944(4)
O(10)	2010(4)	2311(5)	6697(2)
Si(11)	1363(2)	1624(2)	7085(1)
C(12)	1771(8)	2184(12)	7812(4)
C(13)	1504(8)	−97(9)	7074(5)
C(14)	51(6)	2077(8)	6816(4)
C(15)	−46(7)	3471(9)	6745(5)
C(16)	−320(7)	1455(10)	6264(4)
C(17)	−592(7)	1662(10)	7216(5)
O(18)	4312(4)	2808(5)	6153(2)
Si(19)	5350(2)	2129(3)	6115(1)
C(20)	6156(7)	1998(11)	6816(4)
C(21)	5158(7)	578(9)	5805(4)
C(22)	5966(7)	3140(9)	5666(4)
C(23)	6122(7)	4437(11)	5896(4)
C(24)	6977(7)	2613(11)	5642(4)
C(25)	5348(7)	3190(9)	5082(4)
N(26)	3180(5)	678(7)	6265(3)
O(27)	3277(4)	−472(6)	6278(3)
N(28)	3935(5)	2306(7)	7171(3)
C(29)	4051(7)	1255(9)	7470(4)
C(30)	4555(8)	1247(10)	8013(4)
C(31)	4956(7)	2312(10)	8265(4)
C(32)	4851(7)	3343(10)	7959(4)
C(33)	4358(7)	3327(9)	7408(4)
N(34)	2818(5)	4404(6)	6342(3)
C(35)	2442(6)	4941(8)	6742(3)
C(36)	2228(7)	6174(8)	6734(4)
C(37)	2415(7)	6908(8)	6309(4)
C(38)	2800(6)	6364(8)	5904(4)
C(39)	3008(6)	5113(8)	5933(4)

$W_2(\mu\text{-}O)(\mu\text{-}OBu^t)(OSiMe_2Bu^t)_5(py)_2$ (V)

In addition to the W_2-containing complex the asymmetric unit contains one molecule of toluene solvent (C(61) through C(67)). The closest approach between the solvent molecule and the W_2-containing complex is 3.53 Å between C(63) and C(53). The final difference map was essentially featureless. The maximum peaks were 1.45 e/Å^3 at a distance of 0.19 Å from W(2) and 1.38 e/Å^3 at 1.38 Å from W(1). The minimum of the difference map was −1.42 e/Å^3.

$W(NO)(OSiMe_2Bu^t)_3(py)_2$ (IV)

Following complete intensity data collection, a small number of data were removed because of overlapping profiles due to the long *c* axis. After absorption correction, data processing then gave a residual of 0.033 for the averaging of 396 unique intensities which had been observed more than once. Four standards measured every 400 data showed no significant trends. In the final difference map the tungsten residual was 1.36 e/Å^3 and all other residual peaks were less than 0.8 e/Å^3.

TABLE 6. Selected bond distances (Å) and angles (°) for **IV**

Distances	
W(1)–O(2)	1.91(1)
W(1)–O(10)	1.94(1)
W(1)–O(18)	1.97(1)
W(1)–N(26)	1.74(1)
W(1)–N(28)	2.29(1)
W(1)–N(34)	2.34(1)
O(27)–N(26)	1.25(1)
Si–O	1.65 (av)
Angles	
O(2)–W(1)–O(10)	100.1(2)
O(2)–W(1)–O(18)	96.7(2)
O(2)–W(1)–N(26)	100.2(3)
O(2)–W(1)–N(28)	169.4(3)
O(2)–W(1)–N(34)	80.4(2)
O(10)–W(1)–O(18)	152.7(2)
O(10)–W(1)–N(26)	97.8(3)
O(10)–W(1)–N(28)	79.6(2)
O(10)–W(1)–N(34)	79.9(2)
O(18)–W(1)–N(26)	100.2(3)
O(18)–W(1)–N(28)	80.0(2)
O(18)–W(1)–N(34)	81.9(2)
N(26)–W(1)–N(28)	90.3(3)
N(26)–W(1)–N(34)	177.7(3)
N(28)–W(1)–N(34)	89.2(3)
W(1)–O(2)–Si(3)	141.4(4)
W(1)–O(10)–Si(11)	150.3(4)
W(1)–O(18)–Si(19)	136.0(4)
W(1)–N(26)–O(27)	176.6(6)

Results and discussion

Synthesis

$W(O)(OSiMe_2Bu^t)_4(py)$ (II),
$W_2(O)_4(OSiMe_2Bu^t)_4(py)_2$ (III) and
$W(NO)(OSiMe_2Bu^t)_3(py)_2$ (IV)

Burgundy colored, hydrocarbon solutions of $W_2(OSiMe_2Bu^t)_6$ (**I**) were allowed to react with NO (3 equiv.) in the presence of pyridine (5 to 10^4 equiv.) at temperatures from −30 to 22 °C. The following color changes were observed: burgundy to purple (30 min) to brown (1 h) to orange–yellow (3 h). Upon removal of the solvent and sublimation (60 °C, 10^{-4} torr), **II** was isolated as a white, crystalline solid. Compound **III** was obtained upon low temperature crystallization from toluene/ pyridine solutions of the sublimation residue. Further crystallizations from pentane allowed the formation of orange crystals of **IV**. Isolated percent yields of **II–IV** are approximately equal

TABLE 7. Atomic positional parameters ($\times 10^4$) for **V**

Atom	*x*	*y*	*z*
W(1)	3593.6(3)	2724.0(2)	2147.8(3)
W(2)	5334.9(3)	2232.6(2)	2346.7(3)
O(3)	4344(4)	1671(4)	2382(5)
O(4)	4577(4)	3397(4)	1880(5)
C(5)	4705(7)	4198(6)	2137(8)
C(6)	5237(7)	4412(6)	1343(8)
C(7)	5242(8)	4208(6)	3273(8)
C(8)	3722(8)	4755(6)	1940(8)
O(9)	2553(4)	2191(4)	2200(5)
Si(10)	2369(2)	1367(2)	2623(2)
C(11)	3323(7)	876(6)	3789(8)
C(12)	1219(8)	1615(7)	3111(9)
C(13)	2274(7)	604(6)	1550(8)
C(14)	3108(8)	437(7)	1019(8)
C(15)	1373(8)	888(6)	673(8)
C(16)	2196(9)	−181(7)	2027(9)
O(17)	3356(5)	3363(4)	3324(5)
Si(18)	2732(2)	3777(2)	4204(2)
C(19)	2726(8)	2991(7)	5164(9)
C(20)	3294(8)	4536(7)	4920(9)
C(21)	1473(8)	4290(7)	3536(8)
C(22)	876(8)	3690(7)	3153(9)
C(23)	1458(8)	4832(7)	2588(9)
C(24)	1013(9)	4827(8)	4346(10)
O(25)	3012(5)	3079(4)	717(5)
Si(26)	2096(2)	3162(2)	−288(2)
C(27)	972(8)	3252(6)	171(8)
C(28)	2324(8)	2262(6)	−1124(8)
C(29)	1998(7)	4081(6)	−1135(7)
C(30)	1367(8)	4020(6)	−2245(8)
C(31)	1509(8)	4845(6)	−640(9)
C(32)	2966(8)	4144(7)	−1280(9)
O(33)	5749(4)	2275(4)	3887(5)
Si(34)	6302(2)	1885(2)	5077(2)
C(35)	5461(7)	1426(6)	5594(8)
C(36)	7428(7)	1107(6)	5110(8)
C(37)	6621(8)	2686(6)	6021(7)
C(38)	5740(10)	3309(7)	6107(9)
C(39)	7114(8)	2311(7)	7124(8)
C(40)	7305(9)	3098(7)	5597(9)
O(41)	6479(4)	2543(4)	2027(5)
Si(42)	7551(2)	2632(2)	2111(2)
C(43)	8442(7)	1800(7)	2938(9)
C(44)	7756(7)	3557(6)	2785(8)
C(45)	7842(7)	2629(6)	738(8)
C(46)	7221(7)	3360(6)	45(7)
C(47)	8883(7)	2660(6)	830(8)
C(48)	7709(7)	1877(6)	142(7)
N(49)	6139(5)	967(4)	2516(6)
C(50)	5926(7)	438(6)	3136(7)
C(51)	6407(7)	−347(6)	3289(7)
C(52)	7153(7)	−624(6)	2785(8)
C(53)	7365(7)	−96(7)	2132(8)
C(54)	6843(7)	684(6)	2012(8)
N(55)	5014(5)	1993(5)	632(6)
C(56)	5076(7)	2530(6)	−77(7)
C(57)	5000(7)	2382(6)	−1153(8)
C(58)	4821(7)	1656(7)	−1519(8)
C(59)	4745(7)	1103(6)	−791(9)
C(60)	4842(7)	1297(6)	261(7)
C(61)	9963(9)	−1941(8)	3750(10)
C(62)	9758(10)	−1200(9)	4154(11)
C(63)	9719(11)	−506(10)	3616(13)
C(64)	9889(10)	−553(11)	2616(14)
C(65)	10140(10)	−1277(13)	2191(13)
C(66)	10156(10)	−1997(11)	2705(12)
C(67)	9981(10)	−2689(10)	4360(11)

TABLE 8. Selected bond distances (Å) and angles (°) for **V**

Distances	
W(1)–W(2)	2.488(1)
W(1)–O(3)	1.89(1)
W(1)–O(4)	2.15(1)
W(1)–O(9)	1.99(1)
W(1)–O(17)	1.89(1)
W(1)–O(25)	1.90(1)
W(2)–O(3)	1.96(1)
W(2)–O(4)	2.09(1)
W(2)–O(33)	1.95(1)
W(2)–O(41)	2.02(1)
W(2)–N(49)	2.22(1)
W(2)–N(55)	2.20(1)
Si–O	1.64 (av)
Angles	
W(2)–W(1)–O(3)	50.9(2)
W(2)–W(1)–O(4)	52.9(2)
W(2)–W(1)–O(9)	133.6(2)
W(2)–W(1)–O(17)	108.7(2)
W(2)–W(1)–O(25)	110.6(2)
O(3)–W(1)–O(4)	103.3(3)
O(3)–W(1)–O(9)	82.7(3)
O(3)–W(1)–O(17)	120.0(3)
O(3)–W(1)–O(25)	118.0(3)
O(4)–W(1)–O(9)	117.3(2)
O(4)–W(1)–O(17)	89.9(3)
O(4)–W(1)–O(25)	81.5(3)
O(9)–W(1)–O(17)	92.5(3)
O(9)–W(1)–O(25)	90.1(3)
O(17)–W(1)–O(25)	121.9(3)
W(1)–W(2)–O(3)	48.4(2)
W(1)–W(2)–O(4)	55.3(2)
W(1)–W(2)–O(33)	100.4(2)
W(1)–W(2)–O(41)	142.0(2)
W(1)–W(2)–N(49)	126.2(2)
W(1)–W(2)–N(55)	85.7(2)
O(3)–W(2)–O(4)	103.3(3)
O(3)–W(2)–O(33)	96.1(3)
O(3)–W(2)–O(41)	162.9(3)
O(3)–W(2)–N(49)	77.9(3)
O(3)–W(2)–N(55)	82.9(3)
O(4)–W(2)–O(33)	104.1(3)
O(4)–W(2)–O(41)	87.2(2)
O(4)–W(2)–N(49)	169.1(3)
O(4)–W(2)–N(55)	84.9(3)
O(33)–W(2)–O(41)	94.3(3)
O(33)–W(2)–N(49)	86.4(3)
O(33)–W(2)–N(55)	170.9(3)
O(41)–W(2)–N(49)	89.3(3)
O(41)–W(2)–N(55)	84.7(3)
N(49)–W(2)–N(55)	84.6(3)
W(1)–O(3)–W(2)	80.7(2)
W(1)–O(4)–W(2)	71.8(2)
W(1)–O(4)–C(5)	134.7(5)
W(2)–O(4)–C(5)	135.9(5)
W(1)–O(9)–Si(10)	141.4(4)
W(1)–O(17)–Si(18)	155.3(4)
W(1)–O(25)–Si(26)	148.3(4)
W(2)–O(33)–Si(34)	153.7(4)
W(2)–O(41)–Si(42)	162.2(4)
W(2)–N(49)–C(50)	120.9(6)
W(2)–N(49)–C(54)	122.4(6)
W(2)–N(55)–C(56)	119.3(6)
W(2)–N(55)–C(60)	122.7(6)

TABLE 9. Summary of crystal data

	II	III	IV	V
Empirical formula	$C_{29}H_{65}NO_5Si_4W$	$C_{34}H_{70}N_2O_8Si_4W_2$	$C_{28}H_{55}N_3O_4Si_3W$	$C_{44}H_{94}N_2O_7Si_5W_2$; C_7H_8
Color of crystal	colorless	colorless	orange	dark purple
Crystal dimensions (mm)	0.30×0.35×0.40	0.04×0.16×0.40	0.08×0.16×0.32	0.16×0.20×0.26
Space group	$P\bar{1}$	$P\bar{1}$	$P2_1/c$	$P\bar{1}$
Cell dimensions				
Temperature (°C)	−132	−170	−169	−170
a (Å)	17.414(5)	10.708(3)	14.049(3)	14.881(3)
b (Å)	22.679(7)	12.469(4)	10.832(2)	17.245(3)
c (Å)	11.519(3)	10.185(3)	24.807(5)	12.830(2)
α (°)	99.77(2)	107.44(1)		91.20(1)
β (°)	102.15(2)	111.56(1)	102.00(1)	102.23(1)
γ (°)	108.13(1)	90.53(2)		76.34(1)
Z (molecules/cell)	4	1	4	2
Volume (Å^3)	4089.00	1195.75	3692.74	3125.26
Calculated density (gm/cm^3)	1.306	1.548	1.378	1.449
R for merging redundant I	0.055	0.045	0.033	0.039
Molecular weight	804.03	1114.98	765.87	1363.51
Linear absorption coefficient (cm^{-1})	30.300	50.492	33.210	38.941
Scan speed (°/min)	8.0	6.0	6.0	6.0
Scan width (° + dispersion)	1.6	1.8	1.6	1.8
Individual background (s)	4	6	6	6
Total no. reflections collected	12213	3643	5572	14152
No. unique intensities	10707	3133	4807	8183
No. with $F\sigma 0.0$	9853	3065	4455	7704
No. with $F\sigma 3.0$ (F)	8714	2975	4086	7015
No. parameters refined	722	227	353	605
$R(F)$	0.0405	0.0333	0.0404	0.0437
$R_w(F)$	0.0405	0.0343	0.0397	0.0427
Goodness of fit for the last cycle	0.891	1.309	1.114	1.161
Maximum delta/sigma for last cycle	0.002	0.06	0.05	0.02

and account for roughly 80% yield based on tungsten. The gaseous by-products of the reaction were shown to be N_2 and N_2O by mass spectrometry and ^{15}N NMR spectroscopy (from reactions employing $^{15}N^{18}O$).

A high yield synthesis of **IV** was achieved by the reaction of $W(NO)(OBu^t)_3(py)$ with 3 equiv. of $HOSiMe_2Bu^t$ in the presence of additional pyridine (eqn. (3)). The silanolysis of $W(NO)(OBu^t)_3(py)$ in the absence of pyridine yields an intractable, viscous residue. We believe an oligomeric species, $[W(NO)(OSiMe_2Bu^t)_3(py)]_n$, has formed in order to achieve coordinative saturation at the metal center.

$$W(NO)(OBu^t)_3(py) + 3HOSiMe_2Bu^t + py \xrightarrow[\text{pentane}]{22\ ^\circ C} \underset{\textbf{IV}}{W(NO)(OSiMe_2Bu^t)_3(py)_2} + 3HOBu^t \quad (3)$$

$Mo_2(OSiMe_2Bu^t)_6$ (VI)

Hydrocarbon solutions of $Mo_2(OBu^t)_6$ and Bu^tMe_2SiOH (6 equiv.) react at 22 °C to give orange–red $Mo_2(OSiMe_2Bu^t)_6$ (**VI**) and Bu^tOH. Compound **VI**, like **I**, is not subject to dimerization to form $M_4(OR)_{12}$ compounds.

$Mo_2(NO)_2(OSiMe_2Bu^t)_6$ (VII)

When nitric oxide (≥ 2 equiv.) is added to a hydrocarbon solution of **VI**, the orange–yellow compound $Mo_2(NO)_2(OSiMe_2Bu^t)_6$ (**VII**) is obtained as a crystalline solid in 88% isolated yield.

$Mo(NO)(OSiMe_2Bu^t)_3(py)_2$ (VIII)

Toluene solutions of **VII** react with pyridine to form the Lewis base adduct $Mo(NO)(OSiMe_2Bu^t)_3(py)_2$ (**VIII**) as a purple crystalline solid.

Spectroscopic properties

$W(O)(OSiMe_2Bu^t)_4(py)$ (II) and $W_2(O)_4(OSiMe_2Bu^t)_4(py)_2$ (III)

Compounds **II** and **III** show one type of siloxide ligand and one type of pyridine ligand in their respective ^1H NMR spectra, even at −60 °C. These solution data are consistent with the molecular structures observed for **II** and **III** in the solid state. Both **II** and **III** have a sharp IR absorption of medium intensity at 1599 cm^{-1} assigned to the coordinated pyridine ligands. In reactions employing $^{15}N^{18}O$ and **I**, mass spectrometry confirmed the incorporation of the ^{18}O label in **II** and

III, thus establishing the origin of the oxo ligands. IR spectra of the ^{16}O and ^{18}O isotopomers of **II** and **III** did not reveal the expected frequency shift in the 1000–850 cm^{-1} range characteristic for terminal tungsten–oxo stretches [14a]. Very strong O–Si absorptions for the attendant siloxide ligands occur between 960 and 780 cm^{-1} and presumably obscure the expected W–O bands. A band shift is observed in the IR spectrum of **III**, from 536 cm^{-1} for the ^{16}O isotopomer to 507 cm^{-1} for the ^{18}O isotopomer, and is assigned to a W–μO–W stretching vibration [14b].

$W(NO)(OSiMe_2Bu^t)_3(py)_2$ (IV) and $Mo(NO)(OSiMe_2Bu^t)_3(py)_2$ (VIII)

In the ^1H NMR spectrum of **IV** at 22 °C, two types of pyridine ligands are observed, and the broadness of the signals associated with the siloxide ligands indicates dynamic behavior in solution. Spiking the NMR sample with pyridine increased the intensity of the signals of one of the pyridine ligands but did not affect the observed chemical shifts. The same observations were made for **VIII**. Therefore, it appears that the dynamic process occurring for **IV** and **VIII** involves loss of a pyridine ligand in solution. At −60 °C, a ^1H NMR spectrum of **IV** displays a chemical shift pattern consistent with that expected for the solid state structure of **IV**, assuming a virtual mirror plane exists in the molecule making the mutually *trans* siloxide groups chemically equivalent. More specifically, the low temperature spectrum shows two types of pyridine signals, one t-butyl signal of intensity 27 and three methyl signals of intensity 6 each. By symmetry considerations, two t-butyl signals of intensity 18:9 are expected. The one signal in the t-butyl region of intensity 27 is attributed to accidental degeneracy of the signals. The low temperature spectrum of **VIII** shows the same pattern, however, two t-butyl signals are observed and have a 2:1 ratio as expected.

The IR spectrum of **IV** taken as a Nujol mull shows a strong absorption for the nitrosyl ligand at 1542 cm^{-1} which shifts to 1489 cm^{-1} for the $^{15}N^{18}O$ nitrosyl isotopomer. The IR spectrum of a toluene solution of **IV** shows three distinct nitrosyl stretches. This, together with the NMR data for **IV**, suggests **IV** dissociates pyridine in solution. The IR spectrum of **VIII** taken as a Nujol mull has a nitrosyl absorption of 1624 cm^{-1} which shifts to 1560 cm^{-1} for the $^{15}N^{18}O$ isotopomer.

$Mo_2(OSiMe_2Bu^t)_6$ (VI)

Compound **VI** displays one type of siloxide ligand in its ^1H NMR spectrum, even at −60 °C, characteristic of the type of spectrum observed for other known $M_2(OR)_6$ compounds.

$Mo_2(NO)_2(OSiMe_2Bu^t)_6$ (VII)

In the IR spectrum of **VII**, a strong nitrosyl absorption occurs at 1648 cm^{-1} which shifts to 1588 cm^{-1} for the $^{15}N^{18}O$ isotopomer. Compound **VII** is fluxional in solution at 22 °C, but at −40 °C two types of siloxide ligands are observed in a 2:1 ratio. The NMR data are reminiscent of that for $Mo_2(OR)_6(NO)_2$ (R = Bu^t, Pr^i or Np) [15] compounds which have the fused trigonal bipyramidal structure **B**.

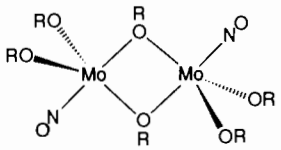

B

Solid-state and molecular structures

$W(O)(OSiMe_2Bu^t)_4(py)$ (II)

There are two independent molecules of **II** in the asymmetric unit, differing with respect to the orientation of the pyridine ligand. Because the molecules are similar, data for only one of the molecules will be discussed in the text with comparison data for both molecules available, see 'Supplementary material'. Atomic positional parameters for **II** are given in Table 1. A ball-and-stick representation of **II** is shown in Fig. 1, with pertinent bond distances and angles provided in Table 2. The $W^{VI}{\equiv}O$ moiety has a bond distance of 1.68 Å as part of a distorted octahedral structure. The bending of the siloxide ligands (oxo–W–OSi angles >90°) away from the oxo ligand is rationalized in terms of repulsive interactions of tungsten–oxo π-bonding with siloxide to

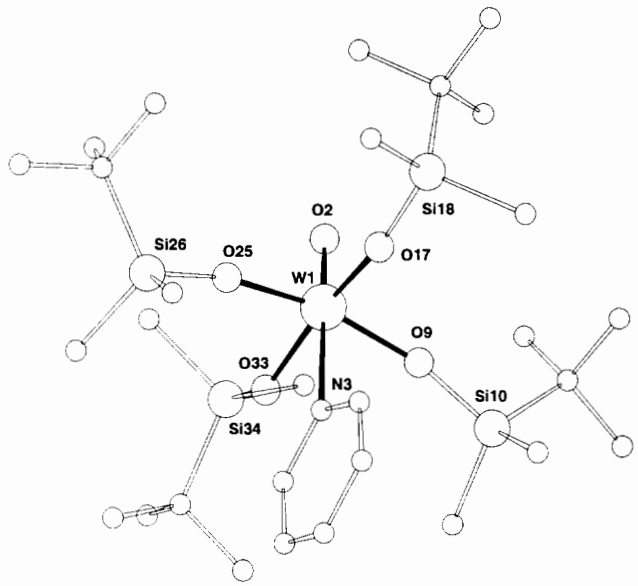

Fig. 1. A ball-and-stick representation for the molecular structure of $W(O)(OSiMe_2Bu^t)_4(py)$ (**II**).

tungsten π-bonding. The *trans* alignment of the pyridine and oxo ligands presumably reflects the *trans* influence order of the ligands (oxo > siloxide > pyridine).

$W_2(O)_4(OSiMe_2Bu^t)_4(py)_2$ (III)

Atomic positional parameters for **III** are listed in Table 3. A ball-and-stick representation of **III** and selected bond distances and angles are given in Fig. 2 and Table 4, respectively. Primes indicate centrosymmetrically related atoms. Compound **III** can be viewed as two $W(O)_2(OSiMe_2Bu^t)_2(py)$ fragments connected through the agency of oxo bridges to give an edge-shared bioctahedral structure. The terminal oxo ligands of each tungsten atom adopt an *anti*-conformation. The siloxide ligands bend away from the tungsten–oxo multiple bond (oxo–W–OSi angles $>90°$), as observed in **II**, presumably due to repulsive π-donor interactions of the siloxide and oxo ligands.

$W(NO)(OSiMe_2Bu^t)_3(py)_2$ (IV)

Atomic positional parameters for **IV** are given in Table 5. The ball-and-stick representation for **IV** shown in Fig. 3 and the bond distances and angles listed in Table 6 exemplify the distorted octahedral geometry about tungsten. The nitrosyl ligand is linear (W–N–O = 177°) and the W–N distance is short (1.74 Å), both indicating multiple bonding between tungsten and nitrogen. One pyridine ligand is *trans* to the nitrosyl ligand and the other is *trans* to a siloxide ligand, with a longer tungsten–nitrogen distance in the former (2.34 versus 2.29 Å). The remaining two siloxide ligands are mutually *trans* and display longer tungsten–oxygen distances (1.95 Å av.) than the siloxide ligand *trans* to pyridine (1.91 Å). These observations reflect a *trans* influence order nitrosyl > siloxide > pyridine.

Compound **IV** adopts a structural type not previously observed for $[W(NO)(OR)_3L]_x$ compounds (structure **C** for R = Bu^t and **D** for R = Bu^i [16]) due to the ligation of an additional donor ligand. We conclude that the

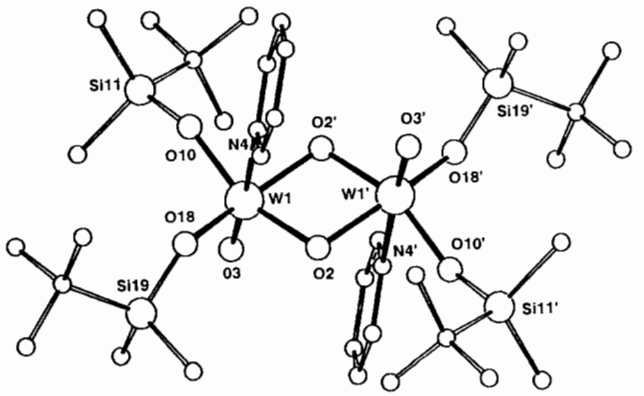

Fig. 2. A ball-and-stick representation for the molecular structure of $W_2(O)_4(OSiMe_2Bu^t)_4(py)_2$ (**III**).

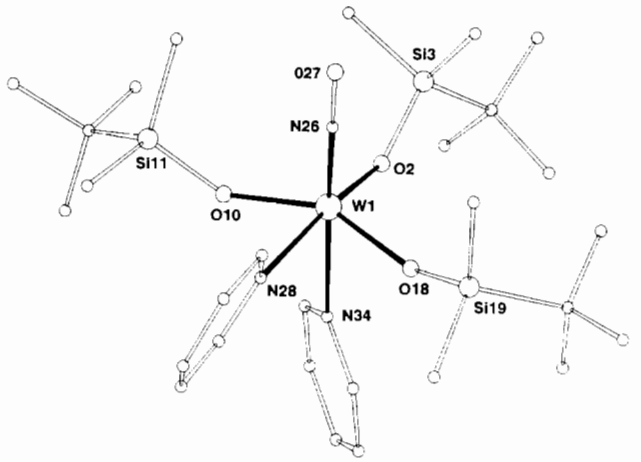

Fig. 3. A ball-and-stick representation for the molecular structure of $W(NO)(OSiMe_2Bu^t)_3(py)_2$ (**IV**).

$OSiMe_2Bu^t$ ligand is less sterically demanding at the metal center than OBu^t. We cannot, however, discriminate between subtle electronic or steric reasons or a combination of the two that cause **IV** to preferentially increase its coordination number at the metal by the addition of pyridine rather than siloxide bridge formation between two $W(NO)(OR)_3(py)$ fragments as observed in structure type **D**.

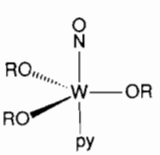

C

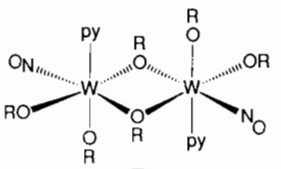

D

$W_2(\mu\text{-}O)(\mu\text{-}OBu^t)(OSiMe_2Bu^t)_5(py)_2 \cdot toluene$ (V)

Atomic positional parameters for **V** are listed in Table 7. A ball-and-stick representation for **V** with the atom labelling scheme is shown in Fig. 4 with selected bond distances and angles given in Table 8. The molecule of toluene solvent contained in the asymmetric unit does not interact with the metal containing fragment of the structure and is therefore not included in Fig. 4.

The two metal atoms share an oxo and t-butoxide ligand via asymmetric bridges and the local geometry about each metal is different. W(2) is octahedrally ligated by an oxo, a t-butoxide, two siloxide and two pyridine ligands. The trigonal bipyramidal geometry of W(1) is formed by the oxo, one t-butoxide and three siloxide ligands. The oxo ligand and two siloxide oxygens (O(17) and O(25)) lie in the equatorial positions of the trigonal bipyramid. The remaining siloxide oxygen and t-butoxide oxygen lie in axial positions. Counting the oxo as a 2-ligand, compound **V** is viewed as containing a $[W_2]^{8+}$ core. This view would allow two d-electrons

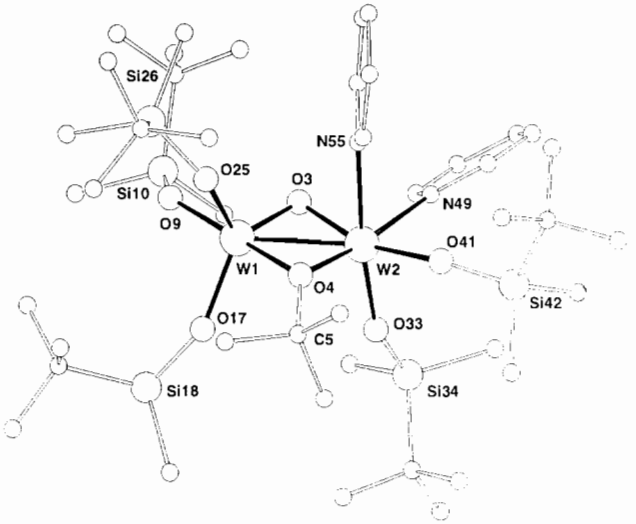

Fig. 4. A ball-and-stick representation for $W_2(\mu\text{-}O)(\mu\text{-}OBu^t)(OSiMe_2Bu^t)_5(py)_2$ (**V**).

per tungsten atom to participate in metal–metal bonding. The short W–W distances of 2.49 Å is consistent with W–W distances observed in other compounds postulated to contain a W–W double bond [17].

Concerning the nature of the reaction between I and NO

The formation of the oxo compounds **II** and **III** is in marked contrast to the preparation of $W(NO)(OBu^t)_3(py)$ as illustrated in eqn. (2). We have reexamined reaction (2) and have found that the formation of $W(NO)(OBu^t)_3(py)$ in high yield (quantitative by ^1H NMR spectroscopy) is independent of the amount of NO (2–10 equiv.) initially added, the reaction temperature (−72 to 25 °C) and the reaction solvent (hydrocarbon/pyridine mixtures). This prompted further investigation into the reaction between the siloxide **I** and NO.

The following observations show that the oxygen atom transfer process occurs under a variety of conditions.

(i) At lower reaction temperatures (−72 °C), the ratio of the oxygen atom transfer compounds **II** and **III** formed relative to **IV** in the reaction of **I** with 3 equiv. NO and pyridine decreased such that the formation of **IV** increased to *c.* 50% yield based on tungsten.

(ii) When the reaction of **I** with 3 equiv. of NO was carried out without pyridine, either in hydrocarbon solutions or in the solid/gas phase, a reaction occurred. Pyridine-d_5/benzene-d_6 (50% vol./vol.) solutions of the reaction residues were analyzed by ^1H NMR spectroscopy and were shown to contain compounds **II**–**IV**. Interestingly, the purple color previously noted in the reaction of hydrocarbon/pyridine solutions of **I** with 3 equiv. NO was not observed, suggesting that an intermediate in the reaction forms a purple colored pyridine adduct. We will later address the identity of this purple colored compound and postulate that it is an intermediate in the reaction pathway leading to the observed oxygen atom transfer products (*vide infra*).

(iii) When **I** was allowed to react with 2 equiv. of NO in the presence of pyridine, ^1H NMR spectroscopy revealed that **II**, **III**, **IV**, unreacted **I** and the purple intermediate were present in the reaction residue. The reaction between **I** and 1 equiv. NO in the presence of pyridine gave **II** and **IV** (no **III**) in relatively smaller amounts when compared to the amount of the purple intermediate and unreacted **I** present in the reaction residue.

By analogy with the reaction shown in eqn. (2), the formation of the tungsten nitrosyl **IV** from **I** would require 2 equiv. of NO. A balanced reaction can be written for the reaction of **I** with 3 equiv. NO and pyridine to form the observed oxo products and N_2 (eqn. (4)). By using a gas manifold, the reaction between **I** and 3 equiv. NO was shown to yield a non-

$$W_2(OSiMe_2Bu^t)_6 + 3NO + 2py \longrightarrow \underset{\textbf{II}}{W(O)(OSiMe_2Bu^t)_4(py)} + \underset{\textbf{III}}{0.5W_2(O)_4(OSiMe_2Bu^t)_4(py)_2} + 3/2N_2 \quad (4)$$

condensable gas. Mass spectrometry identified N_2 as well as N_2O as the gaseous by-products of the reaction. Furthermore, from reactions of **I** with $^{15}N^{18}O$, ^{15}N NMR spectroscopy (^{15}N has $I = 1/2$) allowed the identification of $^{15}N_2$ ($\delta = -70.6$)*, $^{15}N^{15}NO$ ($\delta = -147.1$, -230.5 with $J(NN) = 6$ Hz)** and **IV** ($\delta = 16.2$ $J(W\text{–}N) \leqslant 16$ Hz) as the ^{15}N-containing products of the reaction.

The formation of N_2O in the reaction of **I** with NO indicates that a more complicated reaction sequence is involved in the formation of the oxo compounds than that shown in eqn. (4). We will show later that N_2O itself is capable of reacting with **I** and the purple intermediate.

We have examined the possibility that **IV** is an intermediate in the formation of **II** or **III**, and have found that **IV** does not react with NO, N_2O or **I** to form **II** or **III**. Furthermore, **IV** does not decompose upon heating to 60 °C at 10^{-4} torr (the sublimation conditions for **II**) to give detectable amounts of **II** or

*The chemical shift value was authenticated by ^{14}N NMR spectroscopy; the ^{14}N chemical shift value of $^{14}N_2$ in toluene shows only a slight isotopic shift when compared to the ^{15}N chemical shift value of $^{15}N_2$ [18].

**Values compared to $^{15}N^{15}NO$ chemical shift values previously reported [19].

III. Similar reactions of **II** and **III** with NO and N_2O did not result in the formation of **IV**. Compound **II** did not react further with the oxygen atom sources NO or N_2O to form **III**. These reactions are summarized in Scheme 2. Thus, for the reaction conditions described, it appears that the nitrosyl **IV** is formed in a reaction pathway that is separate from that of the oxo compounds **II** or **III**. The oxo compounds **II** and **III** appear to be formed as coproducts of a reaction (viz. eqn. (4)) because the compounds are observed to form in the expected 2:1 (**II**:**III**) ratio (by ^1H NMR spectroscopy) when **I** is given 3 oxygen atom equivalent.

Reaction of I with N_2O: the purple intermediate

When hydrocarbon/pyridine solutions of **I** were allowed to react with N_2O ($\geqslant 3$ equiv.) at -30 to 22 °C, the burgundy color of the solution changed to purple within 15 min, and then faded to straw yellow after several hours. Compounds **II** and **III** were formed in a 2:1 ratio as determined by ^1H NMR spectroscopy. Thus, the N_2O produced in the reaction of **I** with NO is likely to be involved in the overall reaction sequence that yields **II** and **III**.

The compound giving rise to the purple color in the reaction of **I** with N_2O is the same as that observed in the reaction of **I** with NO (*vide supra*). By allowing hydrocarbon/pyridine solutions of **I** and 1 equiv. of N_2O to react at -72 °C for 1 h, a purple precipitate could be isolated. However, once isolated, the purple solid slowly decomposed at room temperature preventing the use of elemental analysis to determine the chemical composition of the compound. Several samples of the purple solid were submitted for analysis by X-ray crystallography, but in all but one case the crystals did not diffract. From one sample a purple crystal was obtained and characterized by X-ray diffraction as $W_2(\mu\text{-}O)(\mu\text{-}OBu^t)(OSiMe_2Bu^t)_5(py)_2 \cdot$ toluene (**V**). Compound **V** is most likely obtained from the reaction of $W_2(OBu^t)(OSiMe_2Bu^t)_5$ (formed by incomplete silanolysis of $W_2(OBu^t)_6$ in the preparation of **I**) with N_2O. While we cannot conclusively determine that the purple product from the reaction of **I** with N_2O (or NO) is the all siloxy analogue of **V**, the following observations suggest that it is probable. (i) The purple product can be isolated as the major tungsten-containing compound in the reaction of **I** with 1 equiv. N_2O and pyridine, suggesting the product is indeed a mono-oxygen atom species. (ii) Once isolated, the purple product will react with additional N_2O in the presence of pyridine to form **II** and **III**. (iii) In a sealed NMR tube, the purple, benzene-d_6 solution of the compound fades to yellow when stored at 22 °C. ^1H NMR spectroscopy of this yellow solution revealed only **II** in the NMR spectrum. The fate of the remaining '$W(OSiMe_2Bu^t)_2$' fragment is not known.

These observations lead us to believe that the purple intermediate is $W_2(\mu\text{-}O)(\mu\text{-}OSiMe_2Bu^t)(OSiMe_2Bu^t)_5(py)_2$ (the all siloxy analogue of **V**) and is a labile intermediate in the reaction pathway leading to **II** and **III**. The release of **II** from $W_2(O)(OSiMe_2Bu^t)_6(py)_2$ may be oxidatively induced, leaving the coordinatively unsaturated $W(OSiMe_2Bu^t)_2$ fragment capable of accepting two oxygen atoms and pyridine to form **III**. See Scheme 3.

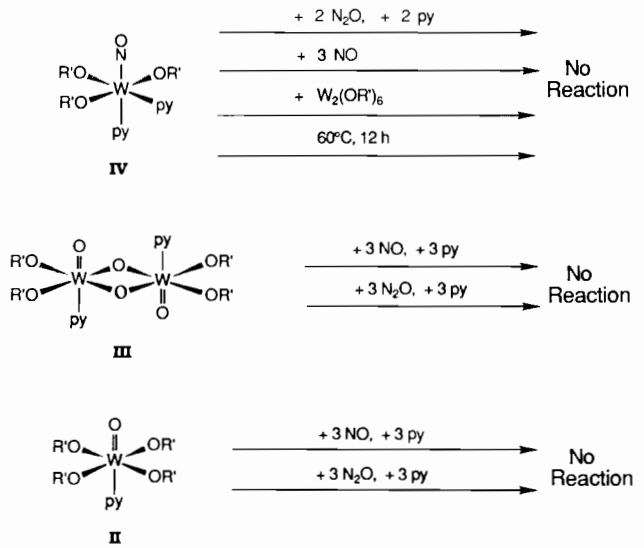

Scheme 2. A summary of the reactions performed which indicate that the nitrosyl compound **IV** and the oxo compounds **II** and **III** are each formed independently. For these reaction conditions each compound is inert with respect to further reactivity. R' = $SiMe_2Bu^t$.

^{15}N NMR spectroscopy

The reaction of **I** with $^{15}N^{18}O$ was followed at -60 °C by ^{15}N NMR spectroscopy. One hour into the reaction, a signal at $\delta = 371$ with coupling to two tungsten atoms ($^1J(WN) = 53$ Hz, intensity = 21%, ^{183}W has $I = 1/2$, 14.7% abundant) as well as the signal for **IV** were observed. The intensity of the signal for **IV** increased over a four hour period. The sample was removed from the probe and the orange–brown solution began turning purple. After allowing the sample to warm for 2 min, the NMR tube was shaken and returned to the -60 °C probe. Upon data collection, the signals for N_2 and N_2O were observed. After storing the NMR sample at 22 °C for 24 h, the signals for **IV**, N_2 and N_2O were observed, but the signal at $\delta = 371$ was no longer detectable.

The signal at $\delta = 371$ is in the chemical shift range previously reported for bridging nitrosyl ligands [20]. Because a $W_2(\mu\text{-}NO)(OSiMe_2Bu^t)_6$ compound is expected to be paramagnetic, it is plausible that a $W_2(\mu\text{-}NO)_2(OSiMe_2Bu^t)_6$ intermediate is responsible for the signal. This leads us to suspect that a bridging bis-

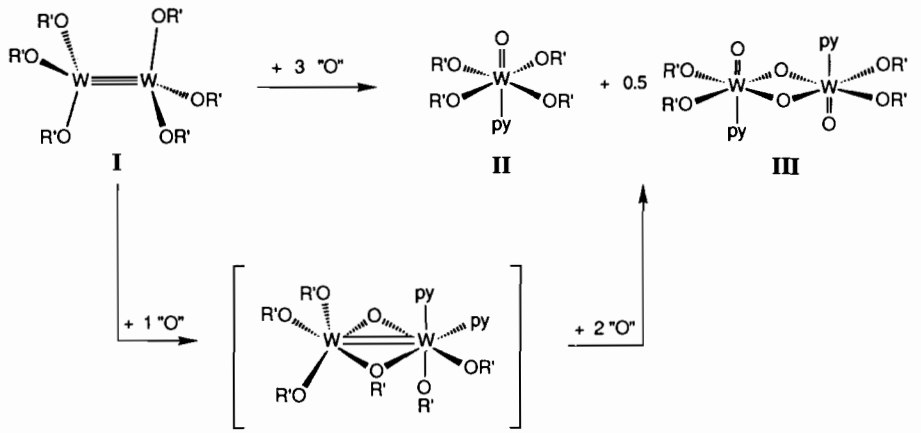

Scheme 3. The role of $W_2(\mu\text{-}O)(OSiMe_2Bu^t)_6(py)_2$ in oxygen atom transfer reactions leading to **II** and **III** from **I**. $R' = SiMe_2Bu^t$.

nitrosyl intermediate could be common to both cleavage of the W=W bond as in eqn. (2) and in N–N bond formation leading to N_2O and the oxo tungsten products **II** and **III**. See Scheme 4.

Comparisons with other work

Nitric oxide has been used to prepare metal–oxo compounds most commonly by decomposition of compounds with nitrosyl ligands or by coupling of two nitrosyl ligands to yield N_2O and a metal oxo. For example, $VICp_2(NO)$ ($Cp = C_5H_5$) slowly decomposes to give $\{[VICp]_2[VCp(NO)]_2(\mu\text{-}O)_4\}$ through an unknown process [21]. The compound $(TiCp_2Cl)_2$ is oxidized by NO to yield $(TiCp_2Cl)_2O$ and N_2O [22]. Paul and Karlin have recently reported the reactions of Cu^I complexes with NO to yield oxo–dicopper(II) complexes and N_2O with spectroscopic evidence indicating a Cu^{II}–$(NO^-)_2$–Cu^{II} intermediate [23]. These results are in agreement with our hypothesis that $W_2(\mu\text{-}O)(OSiMe_2Bu^t)_6(py)_2$ is formed concomitantly with N_2O in the metal-mediated N–N coupling of a $W_2(\mu\text{-}NO)_2$ moiety. Our system is unique in that the ditungsten–oxo formed will react with N_2O to ultimately yield **II** and **III**.

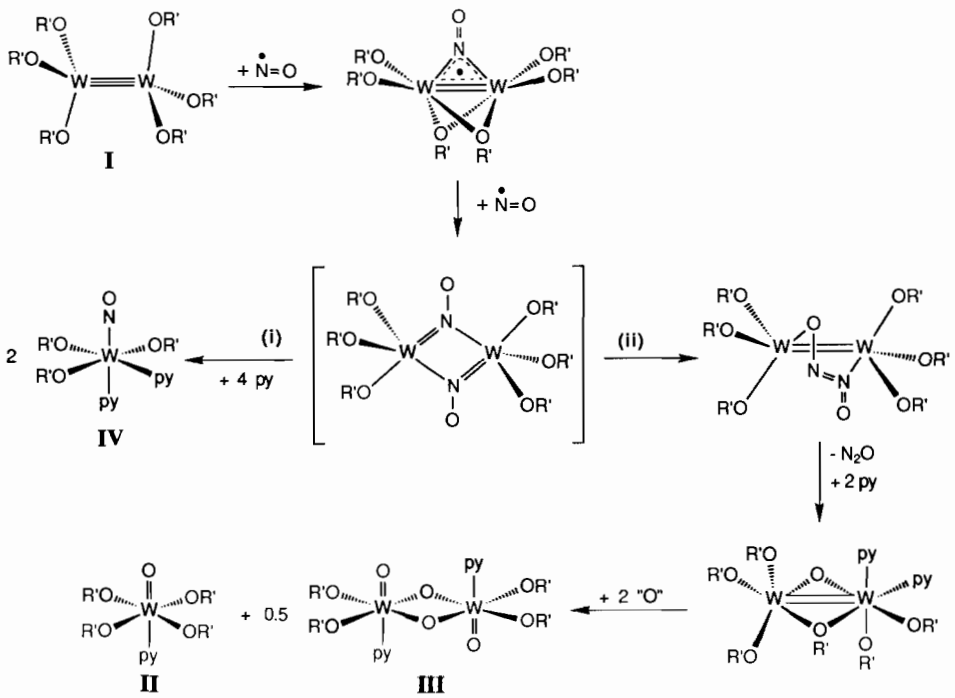

Scheme 4. A proposed reaction sequence leading to a ditungsten–bis-nitrosyl intermediate which could facilitate (i) metal–metal bond cleavage and nitrosyl formation and (ii) N–N coupling to form a hyponitrito ligand which yields $W_2(\mu\text{-}O)(OSiMe_2Bu^t)_6(py)$ and N_2O. $R' = SiMe_2Bu^t$.

Concluding remarks

A direct comparison between the ν(NO) values of W(NO)(OBu^t)$_3$(py) and **IV** is not valid in inferring the relative π-donating ability of the siloxide and alkoxide ligands since the compounds have different structures due to the additional pyridine ligand in **IV**. However, in the structurally related molybdenum compounds, $Mo_2(NO)_2(OBu^t)_6$ and **VII**, the values of ν(NO) are 1625 and 1648 cm^{-1}, respectively. The difference, though small (*c.* 20 cm^{-1}), places the X_3W d_π-to-NO π^* bonding order X = Bu^{t}O > Bu^{t}Me$_2$SiO. This is as expected based on the difference of pK_a values for silanols and alcohols**. Also in a series of $X_3Cr(NO)$ complexes it was found that the value of ν(NO) shifted by *c.* 50 cm^{-1} when X was changed from N(Pr^i)$_2$ (ν(NO) = 1641 cm^{-1}) to N(SiMe$_3$)$_2$ (ν(NO) = 1698 cm^{-1}) [25].

It is evident that the relatively subtle change between the supporting ligands OBu^t and OSiMe$_2$Bu^t causes a significant change in reactivity of the W≡W bond as noted before in its reactions with ethyne and herein with nitric oxide. Though the detailed pathway leading to oxygen atom abstraction in the reaction of **I** with NO is still not known, the reactions outlined in Scheme 4 have certain attractive features. (i) The proposed bridging mono nitrosyl complex $W_2(\mu$-NO)(OSiMe$_2$Bu^t)$_6$ would be closely related to the structurally characterized compounds $W_2(\mu$-CO) and $W_2(\mu$-CN-xylyl) supported by six alkoxide ligands. The latter have been extensively studied and their electronic structures have been investigated by MO calculations [26]. A $W_2(\mu$-NO) analogue would have one additional electron and can be anticipated to give a $W_2(\mu$-NO) radical. Based on the bonding picture for the μ-CO [26a] and μ-CN-xylyl [26b] compounds, this would be in a metal centered M–M bonding orbital. However, we recognize that the ordering of the orbitals and their relative metal–ligand character could change. (ii) The addition of the second NO molecule would generate a diamagnetic $W_2(\mu$-NO)$_2$(OSiMe$_2$Bu^t)$_6$ molecule for which the valence bond description shown in Scheme 4 emphasizes an analogy with alkylidyne and amido chemistry. It is this species that we believe is responsible for the ^{15}N NMR signal at δ 371. (iii) The $W_2(\mu$-NO)$_2$ containing intermediate may then undergo bridge opening and uptake of pyridine to yield **IV**. Alternatively, an intramolecular N–N bond forming reaction would generate a bridging hyponitrito ligand $W_2(\mu$-ONNO). This type of coupling parallels the reversible alkylidyne to bridging alkyne coupling of the type shown in eqn. (1). This has also been observed in other reactions of (RO)$_3$W≡CR′ compounds [27]. The nature of the bridging ONNO ligand would not be expected to parallel that of an μ-alkyne since both N and O coordination are likely as seen in $\{[(NH_3)_5Co]_2(\mu$-ONNO)$\}^{+3}$ [28]. Scheme 4 shows that oxygen atom abstraction from the μ-ONNO ligand could lead to $W_2(\mu$-O)(OSiMe$_2$Bu^t)$_6$(py)$_2$ and N_2O. From here the products **II** and **III** are formed.

**Though the pK_a of Bu^{t}Me$_2$SiOH is not known, that of Et$_3$SiOH has been determined to be *c.* 14 [24a] which compares with 19 [24b] for Bu^{t}OH.

Acknowledgement

We thank the Department of Energy, Office of Basic Research, Chemical Science Division for support.

References

1 (a) M. H. Chisholm, *Acc. Chem. Res., 23* (1990) 419; (b) M. H. Chisholm, *Pure Appl. Chem., 63* (1991) 665.
2 M. H. Chisholm, D. L. Clark, M. J. Hampden-Smith and D. M. Hoffman, *Angew. Chem., Int. Ed. Engl., 28* (1989) 432.
3 M. H. Chisholm, K. Folting, D. M. Hoffman and J. C. Huffman, *J. Am. Chem. Soc., 106* (1984) 6794.
4 M. H. Chisholm, D. M. Hoffman and J. C. Huffman, *J. Am. Chem. Soc., 106* (1984) 6806.
5 M. L. Listemann and R. R. Schrock, *Organometallics, 4* (1985) 74.
6 M. H. Chisholm, K. Folting, C. E. Hammond, M. J. Hampden-Smith and K. G. Moodley, *J. Am. Chem. Soc., 111* (1989) 5300.
7 M. H. Chisholm, C. M. Cook, J. C. Huffman and W. E. Streib, *J. Chem. Soc., Dalton Trans.,* (1991) 929.
8 M. H. Chisholm, F. A. Cotton, M. W. Extine and R. L. Kelly, *Inorg. Chem., 18* (1979) 116.
9 M. Akiyama, M. H. Chisholm, F. A. Cotton, M. W. Extine, D. A. Haitko, D. Little and P. E. Fanwick, *Inorg. Chem., 18* (1970) 2266.
10 M. H. Chisholm, F. A. Cotton, C. A. Murillo and W. W. Reichert, *Inorg. Chem., 16* (1977) 1801.
11 M. H. Chisholm, K. Folting, J. C. Huffman and C. C. Kirkpatrick, *Inorg. Chem., 23* (1984) 1021.
12 G. Germain, P. Main and M. M. Woofson, *MULTAN78 Manual,* University of York, UK, 1978.
13 W. C. Hamilton, *Acta Crystallogr., 12* (1959) 609.
14 (a) W. A. Nugent and J. M. Mayer, in *Metal Ligand Multiple Bonds,* Wiley, New York, 1988; (b) M. Herberhold, W. Kremnitz, A. Razavi, H. Schollhorn and U. Thewalt, *Angew. Chem., Int. Ed. Engl., 24* (1985) 601.
15 M. H. Chisholm, F. A. Cotton, M. W. Extine and R. L. Kelly, *J. Am. Chem. Soc., 100* (1978) 3354.
16 M. H. Chisholm, V. J. Johnston and W. E. Streib, *Inorg. Chem.*, in press.
17 (a) M. H. Chisholm, *Polyhedron, 2* (1983) 681; (b) F. A. Cotton and R. A. Walton, *Multiple Bonds Between Metal Atoms,* Wiley, New York, 1982.
18 J. Mason, in J. Mason (ed.), *Multinuclear NMR,* Plenum, New York, 1987, Ch. 12, p. 335.
19 P. K. Bhattacharyya and B. P. Dailey, *J. Chem. Phys., 59* (1973) 5820.
20 R. E. Stevens and W. L. Gladfelter, *Inorg. Chem., 22* (1983) 2034.

21 F. Bottomley, J. Darkwa and P. S. White, *J. Chem. Soc., Dalton Trans.,* (1985) 1435.

22 F. Bottomley and I. J. B. Lin, *J. Chem. Soc., Dalton Trans.,* (1981) 271.

23 P. P. Paul and K. D. Karlin, *J. Am. Chem. Soc., 113* (1991) 6331.

24 (a) H. Arm, K. Hoshstrasser and P. W. Schindler, *Chimia, 28* (1974) 237; (b) W. K. McEwen, *J. Am. Chem. Soc., 58* (1936) 1124.

25 D. C. Bradley, C. W. Newing, M. H. Chisholm, R. L. Kelly, D. A. Haitko, D. Little, F. A. Cotton and P. E. Fanwick, *Inorg. Chem., 19* (1980) 3010.

26 (a) P. J. Blower, M. H. Chisholm, D. L. Clark and B. W. Eichhorn, *Organometallics, 5* (1986) 2125; (b) M. H. Chisholm, D. L. Clark, D. Ho and J. C. Huffman, *Organometallics, 6* (1987) 1532.

27 M. H. Chisholm, K. Folting, J. C. Huffman and E. A. Lucas, *Organometallics, 10* (1991) 535.

28 B. F. Hoskins and F. D. Whillans, *J. Chem. Soc., Dalton Trans.,* (1973) 607.